

The EUMETSAT
Network of
Satellite
Application
Facilities



O3M SAF

Ozone and Atmospheric
Chemistry Monitoring

ALGORITHM THEORETICAL BASIS DOCUMENT

GOME-2 surface LER product

Product Identifier

Product Name

O3M-89

Surface LER from GOME-2 / MetOp-A

O3M-90

Surface LER from GOME-2 / MetOp-B

L.G. Tilstra

Royal Netherlands Meteorological Institute (KNMI)

O.N.E. Tuinder

Royal Netherlands Meteorological Institute (KNMI)

P. Stammes

Royal Netherlands Meteorological Institute (KNMI)

Document status sheet

Issue	Date	Page(s)	Modified Items / Reason for Change
1.0	18-03-2013	all	first version of document
1.1	23-10-2013	21	added solar eclipse filtering; added appendices A and B
1.2	25-11-2013	all	changes and update after RR/PCR
1.3	12-12-2013	7,12	further changes after RR/PCR
1.4	02-04-2014	all	added O3M-90; update of figures; textual changes
1.5	25-06-2014	11,13	changes and update after DRR
1.6	13-11-2014	7	added heritage section

Contents

1	Introduction	7
1.1	Document purpose and scope	7
1.2	Heritage	7
1.3	GOME-2 surface LER products	7
1.4	Suggested reading material	8
1.5	Abbreviations and acronyms	8
2	Surface reflectivity databases for the UV-VIS	10
2.1	Introduction	10
2.2	Tables	11
3	Algorithm	14
3.1	Scene LER retrieval	14
3.2	Radiative transfer look-up tables (LUTs)	14
3.3	From scene LER to surface LER	15
3.4	Essential input parameters for radiative transfer	20
3.4.1	Ozone	20
3.4.2	Surface height	20
3.5	Input parameters that influence decision-making	20
3.5.1	Snow, permanent ice, sea ice	20
3.5.2	Surface type	21
3.5.3	Absorbing Aerosol Index	21
3.5.4	Solar eclipse flag	21

3.6	Description of the data processor	21
4	Corrections and flags	25
4.1	Cloud contamination for cells over the ocean	25
4.2	Filling missing data	25
4.3	Quality flags	26
5	Instrument degradation	28
5.1	Introduction	28
5.2	Analysis	28
5.3	Correction	30
6	Error analysis	31
7	Proposed validation	32
A	Examples of the monthly GOME-2 surface LER product	33
B	Overview of solar eclipse events	35
	References	37

1 Introduction

1.1 Document purpose and scope

This document is the Algorithm Theoretical Basis Document (ATBD) for the GOME-2 surface LER products developed at KNMI in the framework of the O3M SAF (Satellite Application Facility on Ozone and Atmospheric Chemistry Monitoring). The aim of this ATBD is to present the scientific background of the algorithm and to provide a description of the algorithm setup.

1.2 Heritage

The GOME-2 surface LER product is the Lambertian-equivalent reflectivity (LER) of the Earth's surface observed by GOME-2. It is the improved follow-up of earlier surface LER databases based on observations performed by GOME-1 (on ERS-2) [Koelemeijer *et al.*, 2003] and OMI (on the Aura satellite) [Kleipool *et al.*, 2008]. The GOME-2 surface LER products are developed at KNMI in the framework of the O3M SAF (Satellite Application Facility on Ozone and Atmospheric Chemistry Monitoring). The algorithm described in section 3 of this ATBD is the direct continuation of the algorithms that were developed by Koelemeijer *et al.* [2003] and Kleipool *et al.* [2008].

1.3 GOME-2 surface LER products

Two separate GOME-2 surface LER products will be produced: one derived from level-1 data from GOME-2 onboard MetOp-A, and one from GOME-2 on MetOp-B. To be more specific:

Product ID	Satellite	Platform	Surface LER versions
O3M-89	GOME-2	MetOp-A	MSC & PMD
O3M-90	GOME-2	MetOp-B	MSC & PMD

These GOME-2 surface LER products will each contain two surface LER versions: one version based on GOME-2 observations by the Main Science Channels (MSCs) and one version based on GOME-2 observations by the Polarisation Measurement Devices (PMDs). The PMD-based version has the advantage over the MSC-based version that the surface LER is based on eight times as many observations, each with an eight times smaller footprint. This makes the retrieved surface LER less susceptible to residual cloud contamination, statistically more stable, and therefore more reliable. It also allows a higher spatial resolution of the end product, the surface LER database grid.

On the other hand, the surface LER of the PMD-based version is available only for a fixed list of

wavelength bands. The exact wavelengths of the PMD bands are given in Table 3. This limitation is not an issue for the MSC-based surface LER. Here the wavelengths can be chosen freely (but within the continuum, avoiding absorption bands). The proposed wavelengths are given in Table 2. In this ATBD we do not distinguish between the two approaches, because they are very similar.

1.4 Suggested reading material

Herman, J. R., and E. A. Celarier (1997), Earth surface reflectivity climatology at 340–380 nm from TOMS data, *J. Geophys. Res.*, *102*(D23), 28,003–28,011, doi:10.1029/97JD02074 — HC1997

Koelemeijer, R. B. A., J. F. de Haan, and P. Stammes (2003), A database of spectral surface reflectivity in the range 335–772 nm derived from 5.5 years of GOME observations, *J. Geophys. Res.*, *108*(D2), 4070, doi:10.1029/2002JD002429 — KHS2003

Kleipool, Q. L., M. R. Dobber, J. F. de Haan, and P. F. Levelt (2008), Earth surface reflectance climatology from 3 years of OMI data, *J. Geophys. Res.*, *113*, D18308, doi:10.1029/2008JD010290 — KDHL2008

Popp, C., Wang, P., Brunner, D., Stammes, P., Zhou, Y., and Grzegorski, M. (2011), MERIS albedo climatology for FRESCO+ O2 A-band cloud retrieval, *Atmos. Meas. Tech.*, *4*, 463–483, doi:10.5194/amt-4-463-2011 — POPP2011

1.5 Abbreviations and acronyms

AAI	Absorbing Aerosol Index
ATBD	Algorithm Theoretical Basis Document
BRDF	Bidirectional Reflectance Distribution Function
BSA	Black-Sky Albedo
CDOP	Continuous Development & Operations Phase
DAK	Doubling-Adding KNMI
DU	Dobson Units, 2.69×10^{16} molecules cm^{-2}
EUMETSAT	European Organisation for the Exploitation of Meteorological Satellites
ENVISAT	Environmental Satellite
ERS	European Remote Sensing Satellite
ESA	European Space Agency
ETOPO-4	Topographic & Bathymetric data set from the NGDC, 4 arc-min. resolution
FOV	Field-of-View
FRESCO	Fast Retrieval Scheme for Cloud Observables

FWHM	Full Width at Half Maximum
GOME	Global Ozone Monitoring Experiment
HDF	Hierarchical Data Format
IT	Integration Time
KNMI	Koninklijk Nederlands Meteorologisch Instituut (De Bilt, NL)
LER	Lambertian-Equivalent Reflectivity
LUT	Look-Up Table
MERIS	Medium Resolution Imaging Spectrometer
MLS	Mid-Latitude Summer
MSC	Main Science Channel
NISE	Near-real-time Ice and Snow Extent
NOAA	National Oceanic and Atmospheric Administration
NGDC	NOAA's National Geophysical Data Center (Boulder, Colorado, USA)
NRT	Near-Real-Time
OMI	Ozone Monitoring Instrument
O3M SAF	Satellite Application Facility on Ozone and Atmospheric Chemistry Monitoring
PMD	Polarisation Measurement Device
PSD	Product Specification Document
PUM	Product User Manual
RTM	Radiative Transfer Model
SCIAMACHY	Scanning Imaging Absorption Spectrometer for Atmospheric Chartography
SZA	Solar Zenith Angle
TEMIS	Tropospheric Emission Monitoring Internet Service
TOA	Top-of-Atmosphere
TOMS	Total Ozone Mapping Spectrometer
UTC	Universal Time Co-ordinate
UV	Ultra-Violet
VIS	Visible
VZA	Viewing Zenith Angle

2 Surface reflectivity databases for the UV-VIS

2.1 Introduction

Surface reflectivity databases are needed for cloud, aerosol and trace gas retrievals. One of the first surface reflectivity databases retrieved using UV satellite remote sensing techniques is the Total Ozone Mapping Spectrometer (TOMS) [Heath *et al.*, 1975] surface LER database [Herman and Celarier, 1997]. The retrieved reflectivity is the Lambertian-equivalent reflectivity (LER) of the surface found from scenes which are assumed to be cloud free. The retrieval method relies on the removal of the (modelled) atmospheric contribution from the (observed) top-of-atmosphere (TOA) reflectance. In this approach the surface is defined to behave as a Lambertian reflector. The TOMS surface LER database ($1.25^\circ \times 1^\circ$) was retrieved for 340 and 380 nm only, which limits its usefulness.

The GOME [Burrows *et al.*, 1999] surface reflectivity database provides the surface LER on a $1^\circ \times 1^\circ$ grid for 11 wavelength bands between 335 and 772 nm [Koelemeijer *et al.*, 2003]. Although this is already quite an improvement with respect to the TOMS surface LER database, the database is still limited in quality by the low number of measurements from which the surface LER had to be extracted and the large GOME footprint size (see Table 1). In particular, pixels over sea are often affected by residual cloud contamination. In these cases the surface LER was retrieved from scenes which were not sufficiently cloud free. In other cases, e.g. snow surfaces, the surface LER was retrieved from a few measurements which were not representative for the entire month.

A large improvement on these points is the OMI surface reflectivity database [Kleipool *et al.*, 2008]. First, the OMI instrument [Levelt *et al.*, 2006] has a much smaller footprint size ($24 \times 13 \text{ km}^2$ at nadir) combined with a larger global coverage (see Table 1). This leads to better statistics and results in a higher accuracy for the surface LER retrieval. Second, the higher number of measurements allows for inspecting the distribution of scene LERs for each grid cell, and for making a more sophisticated selection of representative (cloud-free) scenes instead of directly taking the minimum scene LER value like in the case of the TOMS and GOME databases. Third, the provided OMI surface LER database has a higher spatial resolution ($0.5^\circ \times 0.5^\circ$ grid). The limiting factor is the OMI wavelength range. The longest wavelength in the OMI surface LER database is 499 nm.

The GOME-2 series of satellite instruments does not have the limitations of the above instruments and therefore can be used to create a better surface LER database. It has the spectral range of GOME but a much smaller footprint ($80 \times 40 \text{ km}^2$) which is constant over the full swath width. The number of measurements that are available per longitude/latitude cell in the database grid is smaller than that of OMI, but enough to perform a statistical analysis on the distribution of retrieved scene LERs. In this ATBD the approach that was used for the OMI surface reflectivity database is followed closely.

The main advantage of the GOME-2 surface LER database with respect to the OMI surface LER database is the wider wavelength range of the GOME-2 instrument. Additionally, the retrieval algorithm uses aerosol information, available via the GOME-2 Absorbing Aerosol Index (AAI) product, to filter out scenes with large aerosol loadings, as these scenes can result in inaccurate values of the retrieved surface LER. This filtering is especially important for locations over desert areas.

2.2 Tables

In Table 1 we summarise the properties of the discussed surface reflectivity databases. For GOME-2 we provide the specifications for the MSC-based and PMD-based algorithms. In Table 2 we list the wavelength bands of the surface reflectivity databases, and their application. In Table 3 we provide the wavelengths of the GOME-2 PMD bands, relevant to the PMD-based algorithm. The selection of the wavelength bands for the GOME-2 MSC-LER was influenced largely by the already existing surface LER databases. Below 325 nm the surface contribution to the TOA reflectance is low, which prevents an accurate retrieval of the surface LER below this wavelength. For the GOME-2 PMD-LER this means that the surface LER for PMD 1 and 2 cannot be retrieved, as indicated.

instrument	TOMS	GOME	OMI	MSC - GOME-2 - PMD	
satellite	Nimbus-7	ERS-2	Aura	MetOp-A/B	
equator crossing time (LT)	12:00	10:30	13:45	09:30	
dayside flight direction	S→N	N→S	S→N	N→S	
number of days for global coverage	1	3	1	1.5	
pixel size at nadir (km × km)	50 × 50	320 × 40	24 × 13	80 × 40	10 × 40
number of usable pixels per orbit	~12000	~1300	~83000	~11000	~88000
dataset time range (*)	1978–1993	1995–2000	2005–2009	2007→ (*)	2008→ (*)
selected wavelength bands	2	11	23	15	13
wavelength range covered	340–380	335–772	328–499	325–772	325–799
band width (nm)	1.0	1.0	1.0	1.0	see text
spatial resolution (°lon × °lat)	1.25 × 1.0	1.0 × 1.0	0.5 × 0.5	1.0 × 1.0	0.5 × 0.5
reference	HC1997	KHS2003	KDHL2008	this work	

Table 1: Characteristics and properties of the UV-VIS surface LER databases, and of the satellite instruments from which they are derived. Wavelength band information can be found in Tables 2/3.

(*)The longer the time period covered, the higher the number of times a certain region has been observed. This increases the chances of having observed this region under clear sky conditions. Occasional reprocessing over longer time periods therefore increases the quality, stability, and reliability of the surface LER product. GOME-2 data are available from January 2007 (MetOp-A). GOME-2 data from MetOp-B are available since December 2012.

λ (nm)	TOMS	GOME	OMI	GOME-2	application / relevance
325				+	LER, ozone, HCHO, SO ₂
328			+		LER, ozone, HCHO
335		+	+	+	LER, ozone, HCHO
340	+			+	LER, aerosol, HCHO, BrO
342			+		LER, aerosol, HCHO, BrO
345			+		LER, aerosol, HCHO, BrO
354			+	+	LER, aerosol, HCHO, BrO, OCIO
367			+		LER, aerosol, OCIO
372			+		LER, aerosol, OCIO
376			+		LER, aerosol, OCIO
380	+	+	+	+	LER, aerosol, OCIO
388			+	+	LER, aerosol, OCIO
406			+		LER, aerosol
416		+	+	+	LER, aerosol
418			+		LER, aerosol
425			+		LER, aerosol, NO ₂
440		+	+	+	LER, aerosol, NO ₂
442			+		LER, aerosol, NO ₂
452			+		LER, aerosol, NO ₂
463		+	+	+	LER, aerosol, NO ₂ , O ₂ -O ₂
471			+		LER, aerosol, NO ₂ , O ₂ -O ₂
477			+		LER, aerosol, NO ₂ , O ₂ -O ₂
488			+		LER, aerosol, NO ₂ , O ₂ -O ₂
494		+	+	+	LER, aerosol, NO ₂
499			+		LER, aerosol
555		+		+	LER, aerosol
610		+		+	LER, aerosol, H ₂ O
670		+		+	LER, aerosol, H ₂ O, O ₂ -B
758		+		+	LER, aerosol, O ₂ -A
772		+		+	LER, aerosol, O ₂ -A
Total:	2	11	23	15	

Table 2: Wavelength bands of the four monochromatic surface LER databases, and their applications. All wavelength bands are located outside strong gaseous absorption bands in order to avoid complicated modelling of the radiative transfer. The number of wavelength bands is also given.

PMD	λ (nm)	application / relevance	PMD	λ (nm)	application / relevance
01	312	not retrieved	09	460	LER, aerosol, NO ₂ , O ₂ -O ₂
02	317	not retrieved	10	519	LER, aerosol
03	325	LER, ozone, HCHO, SO ₂	11	554	LER, aerosol
04	332	LER, ozone, HCHO	12	589	LER, aerosol
05	338	LER, aerosol, HCHO, BrO	13	639	LER, aerosol, H ₂ O
06	369	LER, aerosol, OCIO	14	756	affected by O ₂ absorption
07	382	LER, aerosol, OCIO	15	799	LER, aerosol
08	413	LER, aerosol			

Table 3: Wavelength information for the PMD bands used in the PMD-based surface LER algorithm. The wavelength definition follows PMD band definition v3.1, so the list applies to MetOp-A PMD data from after 11 March 2008 as well as to all MetOp-B PMD data.

The widths of the PMD bands are not provided in Table 3, but these (and other information) can be found in the “GOME-2 Factsheet” [EUMETSAT, 2014]. For some of the PMD bands the relatively broad wavelength range covered leads to inference with absorption bands. For instance, PMD 14 overlaps with the oxygen-A absorption band and this has affected the retrieved surface LER.

3 Algorithm

3.1 Scene LER retrieval

In the algorithm, we start by calculating the values of the surface albedos that are needed to match simulated reflectances to the measured Earth reflectances. These surface albedos are in fact scene albedos, because they include the effects of surface, clouds, and aerosols. The necessary simulations assume a Rayleigh scattering atmosphere which is bounded below by a Lambertian surface. The contribution of the surface to the top-of-atmosphere (TOA) reflectance may be separated from that of the atmosphere according to the following formula [Chandrasekhar, 1960]:

$$R(\mu, \mu_0, \phi - \phi_0, A_s) = R^0(\mu, \mu_0, \phi - \phi_0) + \frac{A_s T(\mu, \mu_0)}{1 - A_s s^*} \quad (1)$$

In this equation, the first term R^0 is the path reflectance, which is the atmospheric contribution to the reflectance. The second term is the contribution of the surface with an albedo A_s . The parameter T is the total atmospheric transmission for the given zenith angles, s^* is the spherical albedo of the atmosphere for illumination from below, μ is the cosine of the viewing zenith angle θ , and likewise, μ_0 is the cosine of the solar zenith angle θ_0 . Using equation (1) and by demanding that the simulated Rayleigh reflectance R_λ equals the measured reflectance R_λ^{obs} , we find the following expression for the surface albedo A_s , which is a scene albedo, or more specifically, the scene LER A_s :

$$A_s = \frac{R_\lambda^{\text{obs}} - R_\lambda^0}{T_\lambda(\mu, \mu_0) + s_\lambda^*(R_\lambda^{\text{obs}} - R_\lambda^0)} \quad (2)$$

In this equation, R_λ^0 denotes the simulated (path) reflectance at wavelength λ , calculated for the actual atmospheric situation, but without the surface reflection contribution. The path reflectance R^0 can be expanded in a Fourier series. In our case, with a simple Rayleigh atmosphere, this expansion is exact with only three terms in the azimuth angle difference $\phi - \phi_0$:

$$R^0 = a_0 + 2a_1 \cos(\phi - \phi_0) + 2a_2 \cos 2(\phi - \phi_0) \quad (3)$$

The idea of the algorithm setup is that with look-up tables (LUTs) of a_0 , a_1 , a_2 , T , and s^* we can easily calculate R_λ^0 using equation (3) and A_s using equation (2). The advantage of the above approach is that both the azimuthal dependence and the dependence on surface albedo are treated analytically, and are therefore not part of the LUTs. Some interpolation over the remaining parameters is necessary. In this case we have to interpolate over μ and μ_0 , surface height h_s , and ozone column Ω .

3.2 Radiative transfer look-up tables (LUTs)

The look-up tables (LUTs) were created using the radiative transfer code DAK, which stands for ‘‘Doubling-Adding KNMI’’ [de Haan *et al.*, 1987; Stammes, 2001]. This vector radiative transfer

model (RTM) takes polarisation into account, as well as ozone absorption and Lambertian surface reflection. The simulations basically describe a cloud-free, homogeneous atmosphere which is bounded below by a Lambertian surface. We used version 3.1.1 of the DAK RTM. This version supports pseudo-spherical treatment of the Earth's atmosphere. Also, absorption by the O₂–O₂ collision complex is included in the radiative transfer calculations of the LUTs.

The calculations at all wavelengths λ were done for three surface albedos $A_t = \{0.0, 0.5, 1.0\}$, for an azimuth difference $\phi - \phi_0 = 0^\circ$, for 42×42 combinations of the zenith angle cosines μ and μ_0 , for cloud-free conditions in a standard Mid-Latitude Summer (MLS) atmosphere [Anderson *et al.*, 1986], for 7 ozone column values $\Omega = \{50, 200, 300, 350, 400, 500, 650\}$ DU, and for 10 surface heights h_s ranging from 0 to 9 km in 1 km steps. The variation of the surface height was achieved by removing an appropriate number of layers from the bottom of the model atmosphere. Such a removal of layers affects the ozone columns to a (very small) degree, which was compensated for by scaling the entire ozone profile in such a way that the original ozone column value was reinstated.

The coefficients a_0 , a_1 , and a_2 , as defined in equation (3), were delivered directly by the DAK code from the runs with albedo $A_t = 0$. The parameters T and s^* were calculated from the reflectances $R_\lambda(\mu, \mu_0, A_t)$, calculated for the three surface albedos A_t mentioned before, in combination with equation (1). This gives, after some algebra, the following outcome:

$$s_\lambda^* = \frac{R_\lambda(\mu, \mu_0, 1.0) - 2R_\lambda(\mu, \mu_0, 0.5) + R_\lambda(\mu, \mu_0, 0.0)}{R_\lambda(\mu, \mu_0, 1.0) - R_\lambda(\mu, \mu_0, 0.5)}, \quad (4)$$

independent on μ and μ_0 , dependent on surface height h_s , ozone column Ω and wavelength λ , and

$$T_\lambda(\mu, \mu_0) = (1 - s_\lambda^*) \cdot (R_\lambda(\mu, \mu_0, 1.0) - R_\lambda(\mu, \mu_0, 0.0)), \quad (5)$$

which is dependent on μ and μ_0 , surface height h_s , ozone column Ω , and wavelength λ . The LUTs contain the parameters a_0 , a_1 , a_2 , T , and s^* for each of the wavelengths. All parameters except s^* are prepared as a function of μ and μ_0 , surface height, and ozone column. The parameter s^* does not depend on μ and μ_0 , and is given as a function of surface height and ozone column.

3.3 From scene LER to surface LER

Most of the scenes for which we calculate the scene albedo contain clouds or aerosols. The retrieved scene LER A_s is therefore usually not representative for the surface LER. In the minimum-LER (MIN-LER) approach followed in Koelemeijer *et al.* [2003] it is acknowledged that scenes can contain clouds, but the presence of (absorbing) aerosols is neglected. In practice, this means one assumes that the lowest value of the scene LER which is recorded for a certain grid cell on the globe over a sufficiently long period of time (say, one month) is most likely a representative cloud-free scene. The scene LER that was retrieved for the respective observation is then taken as the cell's surface LER.

This MIN-LER approach works well for most surfaces, but it can fail for scenes over snow/ice. For such scenes it is hard to distinguish between the albedo of the snow/ice surface and that of overlying clouds. In the paper by *Kleipool et al.* [2008] a new method is introduced which is based on the analysis of the distribution of the scene LER and/or input from external surface (snow/ice) information. In practice, the method distinguishes between two types of approaches. For most situations the 1% cumulative value of the scene LER is used. This is the mean value of the scene LER that is found from averaging the lowest 1% of the collection of scene LERs. This value is usually very close to the MIN-LER result. For snow/ice surfaces, or for surfaces for which the width of the surface LER distribution is small enough (e.g., desert surfaces), the mode of the distribution is taken.

In this algorithm, we follow roughly the same scheme as was introduced by *Kleipool et al.* [2008]. The flowchart of the process is given in Figure 1. Before describing this flowchart, however, we first explain more about the algorithm setup. The globe is described as a longitude/latitude grid containing cells of 1.0 by 1.0 degree (PMD-LER: 0.5 by 0.5 degree). The GOME-2 measurements are subjected to pre-screening: scenes with high amounts of aerosols are filtered out (section 3.5.3) and scenes which were affected by a solar eclipse are also removed (section 3.5.4).

The many remaining GOME-2 footprints are distributed over the longitude/latitude grid, using the centre longitude and latitude to determine in which cell the measurements belong. For each grid cell the observations collected in one month are processed and only the reflectance in a number of wavelength bands is collected (and corrected for the impact of instrument degradation as explained in section 5). For each grid cell the wavelength band at 670 nm is used to select scenes with the correct scene LER (representative for clear-sky conditions) from all the collected scene LERs [*Koelemeijer et al.*, 2003]. So, the flowchart shown in Figure 1 refers to scene LERs retrieved at 670 nm.

The process starts for each grid cell by determining the total number of observations that were collected in the month that is considered. When this number is less than or equal to 5, then the minimum scene LER value is taken as the surface LER value. At the same time, a flag is raised indicating that the result may be suspicious. Usually, this low number of measurements is an indication that the cell was located at or near the edge of the sunlit part of the globe. In other words, the solar zenith angles of the measurements are very high and for part of the month no observations were found.

For other cases the NISE daily snow/ice database [*Nolin et al.*, 1998] is used to determine whether the measured scenes contained snow, sea ice, or permanent ice. The NISE daily snow/ice database is discussed briefly in section 3.5.1. This snow/ice test is only performed for scenes with latitudes above 5° because the NISE database is less reliable near the equator. Also, near the equator snow/ice is not expected. When the percentage of measurements that were classified as “snow”, “sea ice”, or “permanent ice” is above a certain threshold (10%, 1%, and 20%, respectively), then the mode of the scene LER distribution is used to find the grid cell’s surface LER value [*Kleipool et al.*, 2008].

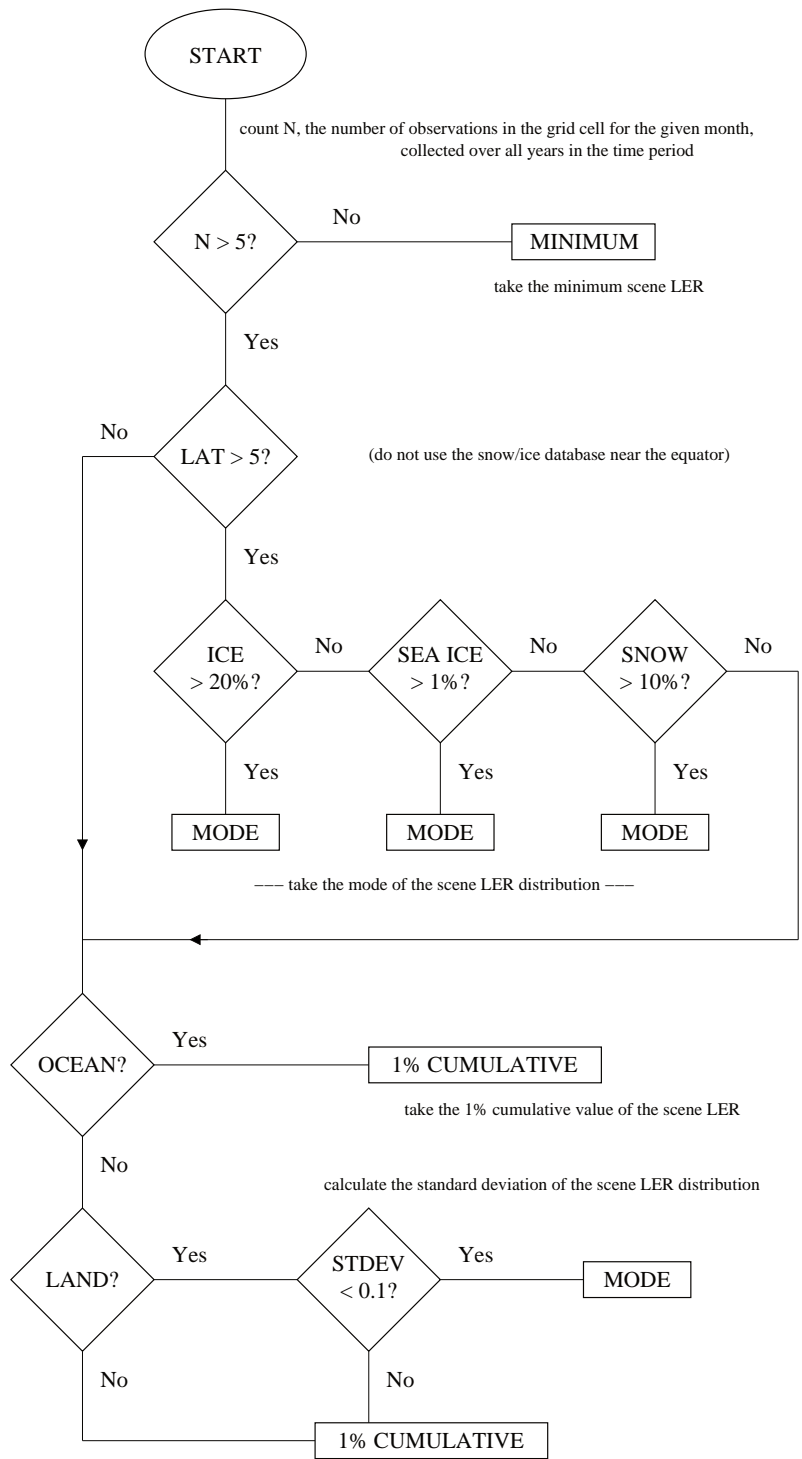


Figure 1: Flowchart describing the process of extracting the surface LER for a certain grid cell from the collected observed scene LER values. More details are provided in the main text.

For the other (remaining) cases the surface type (land/water) is determined from a GTOPO30 surface type database. This database is discussed in section 3.5.2. When the cell is classified as “water” then the 1% cumulative value is taken for the cell’s surface LER. When the cell is classified as “land” then first the standard deviation of the distribution of the scene LER is calculated. If this standard deviation is below 0.1 then the area is considered to be a typical arid desert area and the mode of the scene LER distribution is used to find the grid cell’s surface LER value [Kleipool *et al.*, 2008]. If the standard deviation exceeds 0.1 then the 1% cumulative value is taken for the cell’s surface LER. If at this point the cell has not been assigned a processing strategy, it is assumed to cover a coastal area and the 1% cumulative value is taken for the cell’s surface LER.

In Figure 2 we present, as an example, a global overview of the modes that were used to determine the surface LER for the month May. The data were collected from the years 2007–2013. From the figure it is clear that the desert areas are correctly identified as arid areas. For these scenes the mode LER is used. The minimum-LER approach is used for a small number of measurements. The 1% cumulative value is mostly used. Because of the small number of measurements inside a grid cell (say, 100 measurements for a month of data when 4 years are taken into account), in practice the 1% cumulative value is very similar or completely identical to the minimum-LER value. For that reason, from now on MIN-LER refers to the approach where we use the 1% cumulative value, and MODE-LER refers to the approach where we follow the scheme shown in Figure 1.

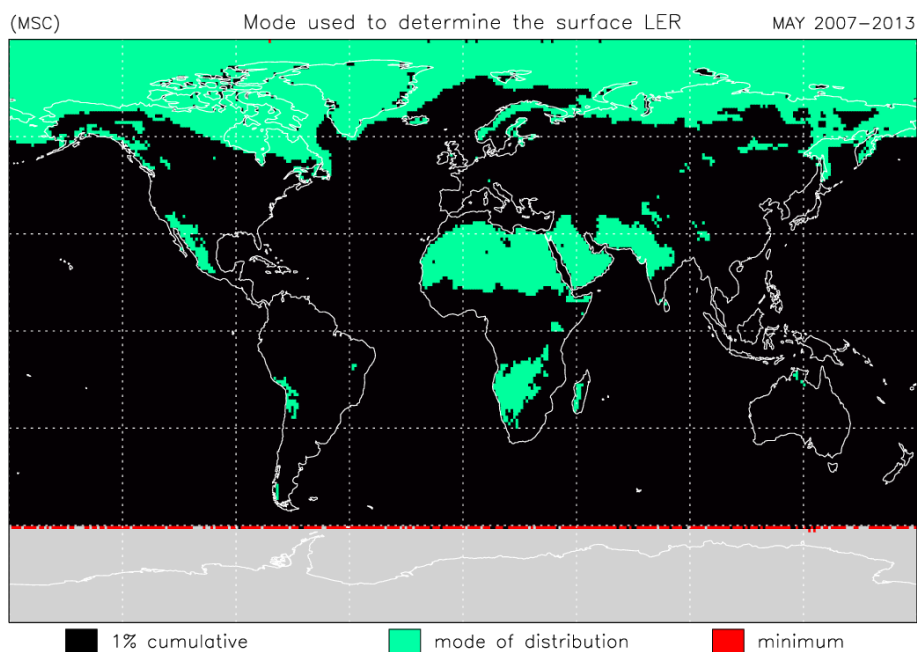


Figure 2: Map indicating where the GOME-2/MetOp-A surface LER algorithm uses the 1% cumulative value (black), the mode of the distribution (green), or the minimum value (red). The data are from the month May. In the grey areas no suitable measurements could be collected ($\theta_0 > 85^\circ$).

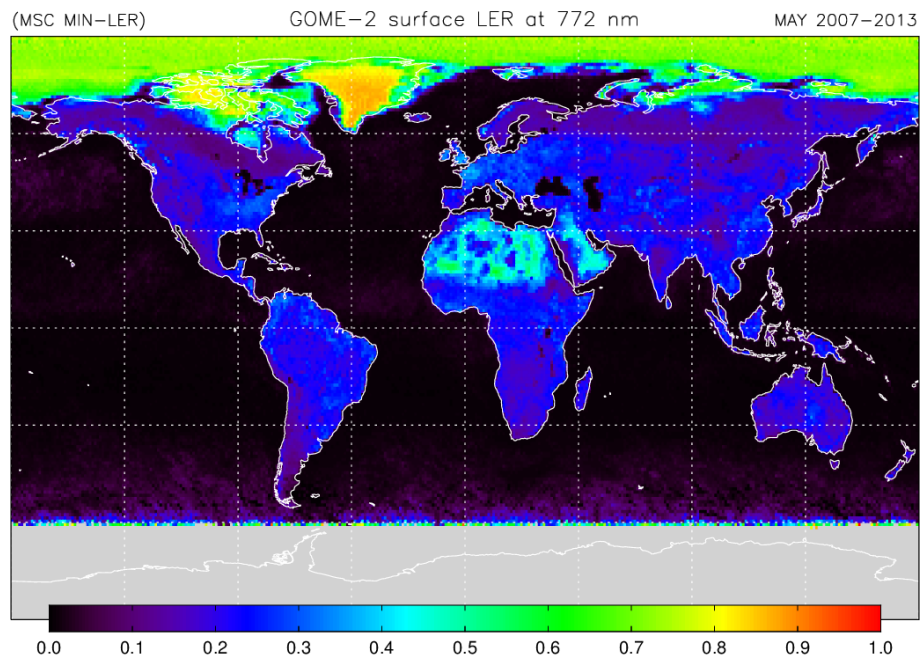


Figure 3: Example of the GOME-2/MetOp-A surface *LER* for the month May, retrieved for 772 nm using the MIN-*LER* approach. The data were collected from the years 2007-2013.

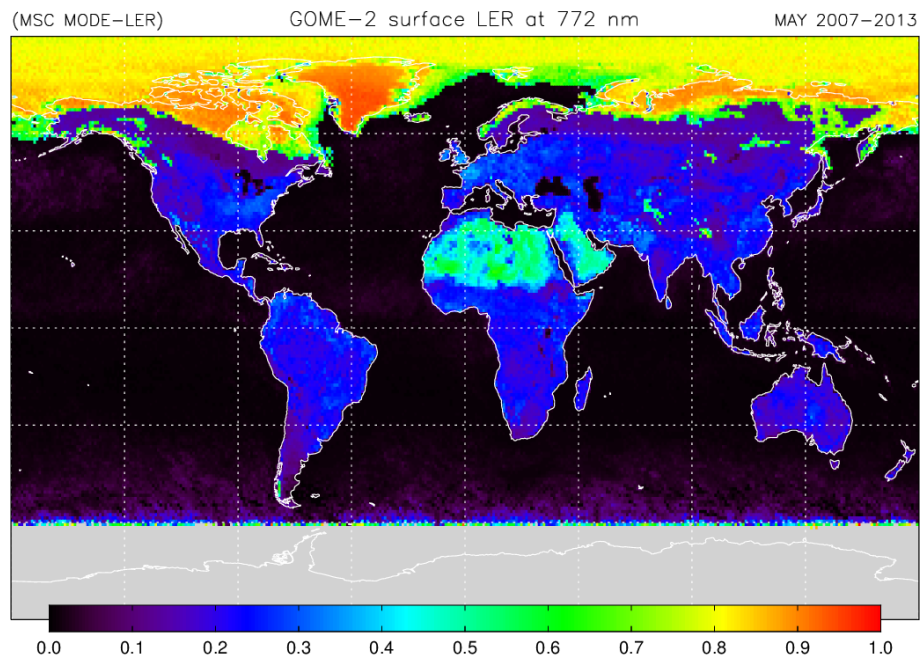


Figure 4: Example of the GOME-2/MetOp-A surface *LER* for the month May, retrieved for 772 nm using the MODE-*LER* approach. The data were collected from the years 2007-2013.

As an example of the GOME-2 surface LER product, we present in Figure 3 the surface LER in the month May retrieved from GOME-2 observations at 772 nm. The approach used here was the MIN-LER approach, and the data were taken from the month May of the years 2007–2013. To compare, in Figure 4 the same result is given for the MODE-LER approach. Obviously, there are large differences for the known snow/ice areas and over the arid (desert) areas. The GOME-2 surface LER products will provide both the MIN-LER and the MODE-LER surface LER result.

3.4 Essential input parameters for radiative transfer

3.4.1 Ozone

Knowledge of ozone column at the measurement footprint is essential for wavelengths below ~ 330 nm and between 450–650 nm, where ozone absorption has a large impact on the reflectance. We use GOME-2 assimilated total ozone columns as input for the radiative transfer calculations. Please note that at the other wavelengths (including 670 nm) absorption by ozone is of much less importance.

3.4.2 Surface height

The mean surface height for each suitable measurement footprint is determined using a high-resolution surface height database. This surface height database was constructed from an ETOPO-4 elevation database [*National Geophysical Data Center, 2006*], and has an angular resolution of 4 arc-minutes in both latitude and longitude. As we are only interested in the topographic information, all bathymetric information was removed from the database, and replaced by a zero surface height. The mean surface height for each footprint is calculated by first determining the grid points of the surface height database that fall inside the footprint, and then averaging their associated surface heights.

3.5 Input parameters that influence decision-making

3.5.1 Snow, permanent ice, sea ice

To determine whether or not a scene is located over snow/ice surfaces, we make use of the “Near-Real-Time SSM/I-SSMIS EASE-Grid Daily Global Ice Concentration and Snow Extent” product, also known as the “Near-real-time Ice and Snow Extent” (NISE) product [*Nolin et al., 1998*]. The daily data are used to find for each GOME-2 measurement footprint the snow/ice situation. When the NISE data for a certain day are not available, then the data from the next day are used.

3.5.2 Surface type

The surface type could in principle be deduced directly, at no extra cost, from the NISE data. Additionally, the NISE data also indicate whether or not a pixel covers a coastal area. Nevertheless, it was decided to determine the surface type from a GTOPO30 surface elevation database. The derived surface type indicator can have the value 0 (for “water”) or 1 (for “land”).

3.5.3 Absorbing Aerosol Index

The Absorbing Aerosol Index (AAI) is calculated within the processing chain. This does not slow down the processing much and has the advantage that there is always absorbing aerosol information available. The algorithm used for the calculation of the AAI is identical to the GOME-2 AAI retrieval algorithm. Details about the GOME-2 AAI retrieval can be found in *Tilstra et al.* [2010].

The AAI is needed to be able to exclude scenes with large concentration of absorbing aerosols. The presence of these aerosols (usually found over cloud-free desert areas in the months June–September) will influence the scene LER and will therefore corrupt the retrieved surface LER. In the code, we filter out all observations for which $AAI > 1$ before analysing the scene LER distribution.

3.5.4 Solar eclipse flag

Solar eclipse events lead to abnormally low values for the retrieved Earth reflectance. Observations taken during a solar eclipse should not be used and the affected measurements need to be removed from the analysis. For the purpose of doing that, a solar eclipse flag is determined for each observation. The derived solar eclipse flag can have the value 0 (“not affected”) or 1 (“affected”). The flag is set according to the information given in Tables 5 and 6 of Appendix B.

3.6 Description of the data processor

The data processor was built as a series of steps which deliver intermediate products which are then used by the next step in the process. A graphical representation of the data processor is given in Figure 5. The input consists of GOME-2 level-1b orbits (or PDUs) of version 5.3 and above. In the first step of the process the Earth reflectance is calculated for all suitable measurements. Whether or not a measurement is “suitable” is determined by the following check list:

1. Is $\theta_0 < 85^\circ$?
2. Is the integration time (IT) 187.5 ms? [24 measurements inside each forward scan]

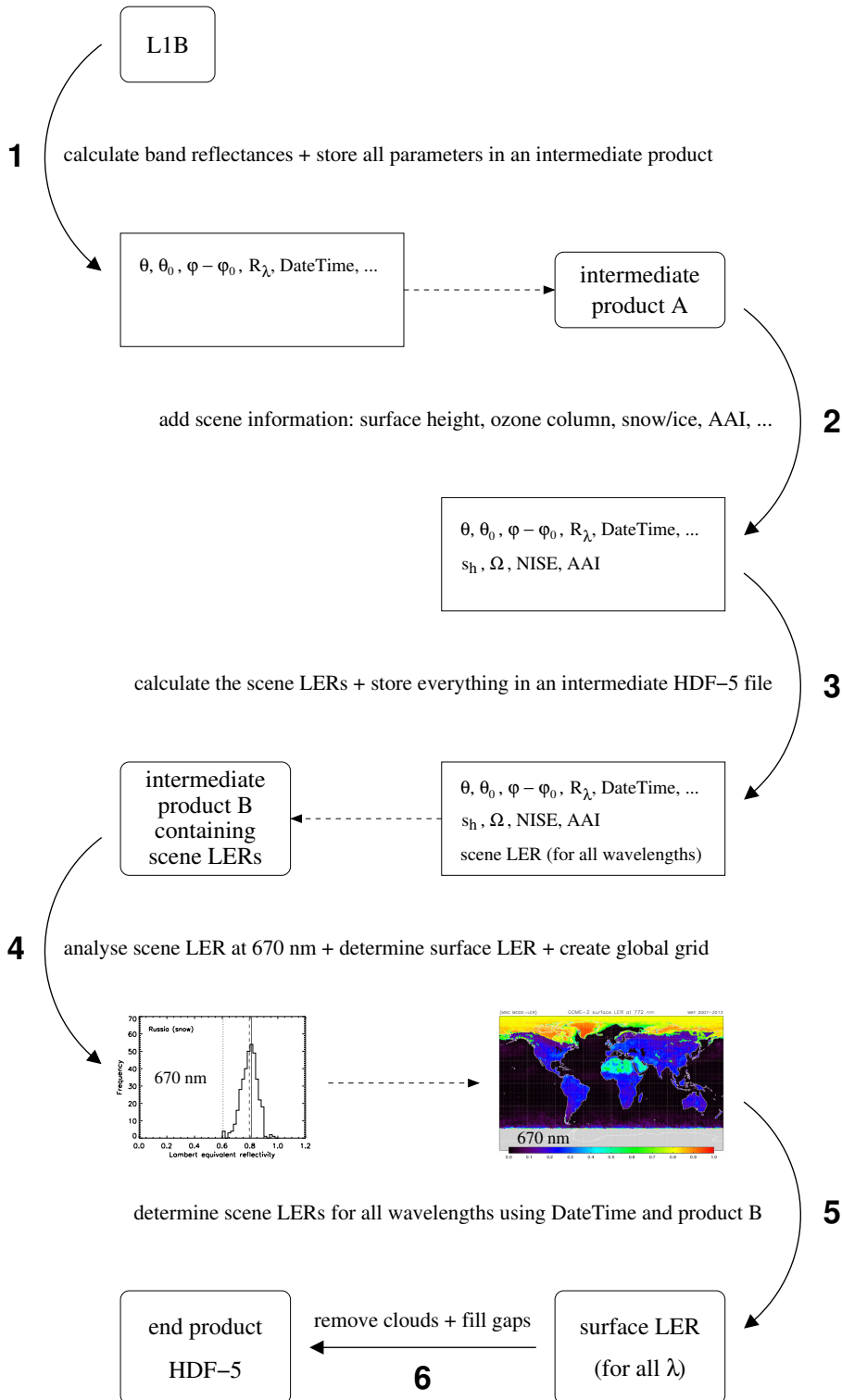


Figure 5: Schematic overview of the six steps that make up the GOME-2 surface LER data processor.

3. Is the measurement from the forward scan? [backscan measurements are not used]
4. Is the measurement from the descending orbit part?
5. Is the measurement not a PMD RAW mode measurement?
6. Does the Earth reflectance show a physical value? [sanity checking]
7. Is the measurement not affected by a solar eclipse event?

Check number “7” is coded manually, which is robust and manageable as solar eclipse events are relatively scarce. From the Earth reflectance spectrum the code calculates the mean reflectance for a predefined list of wavelength bands. The following parameters are stored in intermediate files “A”:

level1_orbit	the filename of the level-1b orbit
level1_version	the processor version of the level-1b orbit
observation_mode	the measurement mode
narrow_swath	indicator for narrow swath / nadir static mode
$\theta, \theta_0, \phi - \phi_0$	viewing and solar angles
λ	list of selected wavelength bands
R_λ	banded Earth reflectances
DateTime	required for finding original observations
centre latitude/longitude	required for gridding and for solving date line problems
corner latitude/longitude	required for e.g. surface height calculation
Index_In_Scan	can be used for e.g. removing scan-angle dependencies
cloud fraction	can be used for e.g. pre-filtering
cloud pressure/height	for distinction between snow/ice and clouds – not used
cloud albedo	not used

These parameters are determined for each PDU or orbit of a certain day, and stored into a file which is placed into a directory structure YYYY/MM/DD. This level-1 extraction is very time consuming and therefore this step of the process does not perform any retrieval steps that might change in the future as the algorithm evolves. The amount of data generated this way amounts to 1.2 Gb per month per year. This completes the description of step “1” of the surface LER data processor.

In step “2” we gather scene information: surface height and type, ozone column, snow/ice information, and AAI (all explained in section 3.4). In step “3” we apply a correction for instrument

degradation (explained in section 5) and determine the scene LER using the theory in section 3.1. Steps “2” and “3” are both executed by the same computer code, which at the end produces intermediate products “B” (in HDF-5 format) containing also the additional parameters.

Step “4” focuses on one wavelength: 670 nm. The scene LER at this wavelength is used to determine which scenes are considered representative for cloud-free situations for which the scene LER corresponds to the surface LER. For each grid cell the code stores the date and time of the representative measurements. See section 3.3. Narrow swath observations are skipped in this step.

In step “5” the code uses the DateTime to calculate the surface LER for all wavelengths. This is done by accessing the intermediate HDF-5 files that were produced in step “3” and averaging the scene LER values of the respective wavelength band. Step “4” and “5” are combined into one computer code. The result is an intermediate file which contains the surface LER grid for all wavelengths for the given month, but also other relevant parameters such as the mode that was used, the number of observations per grid cell, the NISE grid, the estimated errors, et cetera.

The surface LER grids in these intermediate files are not ready to be used. First, some of the grid cells over the ocean need to be corrected for what we call cloud contamination. This phenomenon, caused by persistent cloud presence, is explained more clearly in section 4.1. The actual correction for cloud contamination over the oceans is performed in step “6” of the data processor. Note that the surface LER grids inside the intermediate files are only filled for the sunlit part of the globe (for which $\theta_0 < 85^\circ$, see Figure 2). To offer the users of the GOME-2 surface LER product also meaningful data for these missing parts of the globe, grid cells with no data are filled with surface LER values from other months for which the grid cell did contain a trustworthy value. The exact approach followed is discussed in section 4.2. This correction is also performed in step “6” of the data processor.

This last step in the process not only corrects for cloud contamination and handles missing data, but also provides a quality flag and combines the result for the individual months into one HDF-5 file. This completes the description of the surface LER data processor.

4 Corrections and flags

4.1 Cloud contamination for cells over the ocean

For grid cells located over the oceans, the data processor is constantly looking for cloud-free scenes from which to determine the surface LER. Sometimes, for certain grid cells, and despite having more than six years of data available, a cloud-free scene is never observed. This happens for regions which are known to be suffering from persistent clouds. Figure 6a presents the minimum FRESCO cloud fraction for each grid cells on the world map. As can be seen, the minimum cloud fraction is close to zero for most of the cells, but for some of the cells, this zero value is not reached. For these cells, the retrieved surface LER is contaminated by the influence of clouds. A correction is needed.

In the data processor, we correct for this effect by looking for donor cells which were not cloud contaminated. The process starts with identifying the contaminated cells. This was initially done by looking at the minimum cloud fraction. However, this approach was abandoned because the (FRESCO) cloud fraction used here uses the GOME-1 surface LER database. This is not an independent source, and it is also suffering from cloud contamination. Also, for the PMD measurements no cloud fraction information is currently available. Note that the need for this correction is somewhat smaller for the PMD-LER because of the smaller footprint size of the PMD measurements.

In step “6” of the data processor, we use the retrieved 772-nm surface LER (PMD-LER: PMD 15) in combination with a threshold to find the cloud contaminated grid cells (over the ocean). This seems to work better than using the cloud fraction. The correction is performed for each of the contaminated cells by finding a donor cell in the vicinity of the contaminated cell. This donor cell is searched in a box around the contaminated cell with dimensions of 10° latitude and 30° longitude. However, for contaminated cells in the region near the equator where the absolute latitude is less than 30°, the longitude range of the box is extended to 60°. The donor cell is the cell in the box with the lowest retrieved 772-nm surface LER. The effect of the correction is demonstrated by Figure 6c.

4.2 Filling missing data

Missing data only occurs for grid cells near the polar regions for which the GOME-2 observations (with $\theta_0 > 85^\circ$) were deliberately filtered out. Although the demand for a surface LER value for these geometries seems to be small, some meaningful value should be provided to the users of the data. For that reason, we look for the closest month which does have reliable data for the grid cell in question. We record the surface LER from this donor cell but also its NISE characterisation. We compare the NISE characterisation of the empty cell with the NISE characterisation of the donor cell. When they are identical, then we adopt the surface LER value. When they are not identical, then we

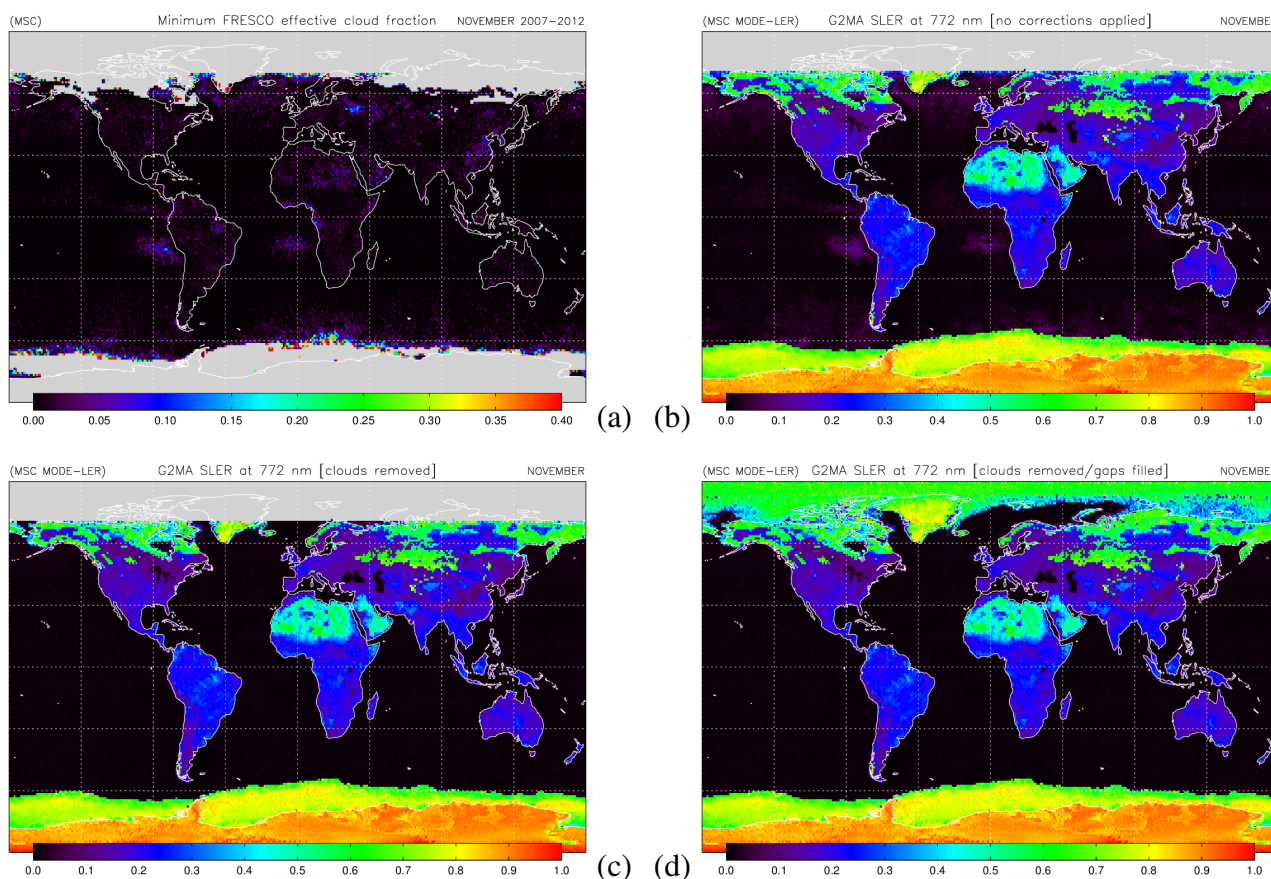


Figure 6: Some intermediate processing results for the month November, determined over the years 2007–2012. (a) Minimum cloud fraction encountered. (b) Surface LER map showing residual cloud structures. (c) Surface LER map after correction for persistent clouds. (d) Surface LER map after filling the gaps near the polar regions with data from other months.

jump to the next month which does have reliable data for the grid cell in question and try again. The filling of missing data in step “6” of the data processor is demonstrated in Figure 6d.

4.3 Quality flags

The quality flags of the surface LER grids are determined mainly by the two correction methods described in this section. The meaning of the flags is given in Table 4. The definition of the quality flag was taken over directly from the paper by *Koелеmeijer et al.* [2003]. Normal, non-corrected grid cells have their flag set to zero. The surface LER data for these cells are expected to be highly reliable. For grid cells above sea, the flag may be set to 1 or 2. When the flag is set to 1, this means that the grid cell was classified as cloud contaminated. The surface LER is the surface LER of a nearby donor cell. The surface LER may still be used as it is expected to be reliable. When the flag is set to 2,

Flag	Meaning of flag
0	data are ok; no corrections applied
1	residual cloud contamination above ocean detected – replaced by nearby cloud-free cell
2	residual cloud contamination above ocean detected – no suitable replacement could be found (the pixel remains cloud contaminated or receives the LER spectrum of a non-representative donor cell)
3	missing data for polar regions which are observed only part of the year – filled in using nearest month with reliable surface LER data
4	missing data throughout the entire year
5	suspect surface LER value retrieved for at least one of the wavelengths

Table 4: Definition of the quality flag that are provided along with the surface LER products.

a replacement could not be found, or the replacement itself was not representative. In this case, the surface LER may still be used but it is expected to be less good.

When the flag is set to 3, the grid cell was not part of the sunlit portion of the Earth for the entire month. Or, more specifically, the number of measurements in the grid cell was below 7 (PMD-LER: 56). In this case, the data processor looks for replacements in neighbouring months.

The flag is set to 4 when no replacement could be found in the entire year. However, this does not happen very often in practice. The flag is set to 5 when the retrieved surface LER for at least one of the wavelengths larger than 325 nm (PMD-LER: PMD 3) is suspect. This may be because the surface LER value found was negative, or because it was found to be larger than what may be expected from a surface LER value. This happens mostly near the polar regions.

5 Instrument degradation

5.1 Introduction

Instrument degradation is a serious problem which strongly affects the Earth reflectance measurements performed by GOME-2 in the UV wavelength range [Tilstra *et al.*, 2012b]. As a result, it also has an impact on the retrieved surface LER values in the UV. The method for in-flight degradation correction that we use has been introduced earlier in Tilstra *et al.* [2012a] for the SCIAMACHY instrument. The method was later applied to the GOME-2 instrument [Tilstra *et al.*, 2012b].

5.2 Analysis

The method is based on studying time series of the daily global mean reflectance. The daily global mean reflectance, denoted by R^* , is defined as the mean of all measured Earth reflectances for a certain scan mirror position on a certain day between 60°N and 60°S and solar zenith angles θ_0 less than 85 degrees. In Figure 7 we present two plots taken from Tilstra *et al.* [2012b] which show the daily global mean reflectance as a function of time for the GOME-2 instrument.

The time series of the global mean reflectance show seasonal variations as well as trends due to instrument degradation. To analyse the time series, we assume that the global mean reflectance may be well described empirically by a function made up of a polynomial term, representing the reflectance change due to instrument degradation, multiplied by a term periodic in time that represents the normal seasonal variation of the global mean reflectance. In other words,

$$R_{\lambda,s}^* = P_{\lambda,s}^{(p)} \cdot [1 + F_{\lambda,s}^{(q)}], \quad (6)$$

where the term P represents the polynomial part of degree p , defined by

$$P_{\lambda,s}^{(p)}(t) = \sum_{m=0}^p u_{\lambda,s}^{(m)} \cdot t^m, \quad (7)$$

while the seasonal variation F is described by a finite Fourier series of order q , according to

$$F_{\lambda,s}^{(q)}(t) = \sum_{n=1}^q [v_{\lambda,s}^{(n)} \cdot \cos(2\pi nt) + w_{\lambda,s}^{(n)} \cdot \sin(2\pi nt)]. \quad (8)$$

In these equations, the parameter t is the time expressed in years since the beginning of the time series (which is 4 January 2007 in the case of GOME-2 on MetOp-A). The parameter λ refers to the wavelength being studied and the integer s relates to the scan mirror position. For GOME-2, this integer runs from 1 to 32 for the nominal integration time (IT) of 187.5 ms when the instrument scans

from east to west and back. Backscan measurements are not considered. Therefore, s effectively runs from 1 to 24. For the present baseline, we use $p = 3$ and $q = 6$.

The polynomial part P is the most important as it represents the relative change in the GOME-2 measured Earth reflectance over the years, per scan mirror position, due to instrument degradation. Normalisation of P immediately leads to the reflectance degradation factor:

$$d_{\lambda,s}(t) = P_{\lambda,s}^{(p)}(t) / P_{\lambda,s}^{(p)}(0) . \quad (9)$$

For GOME-2 the reflectance degradation factor is growing with time for most wavelengths, and is strongly dependent on scan mirror position. Figure 7 shows the behaviour for 325 and 380 nm.

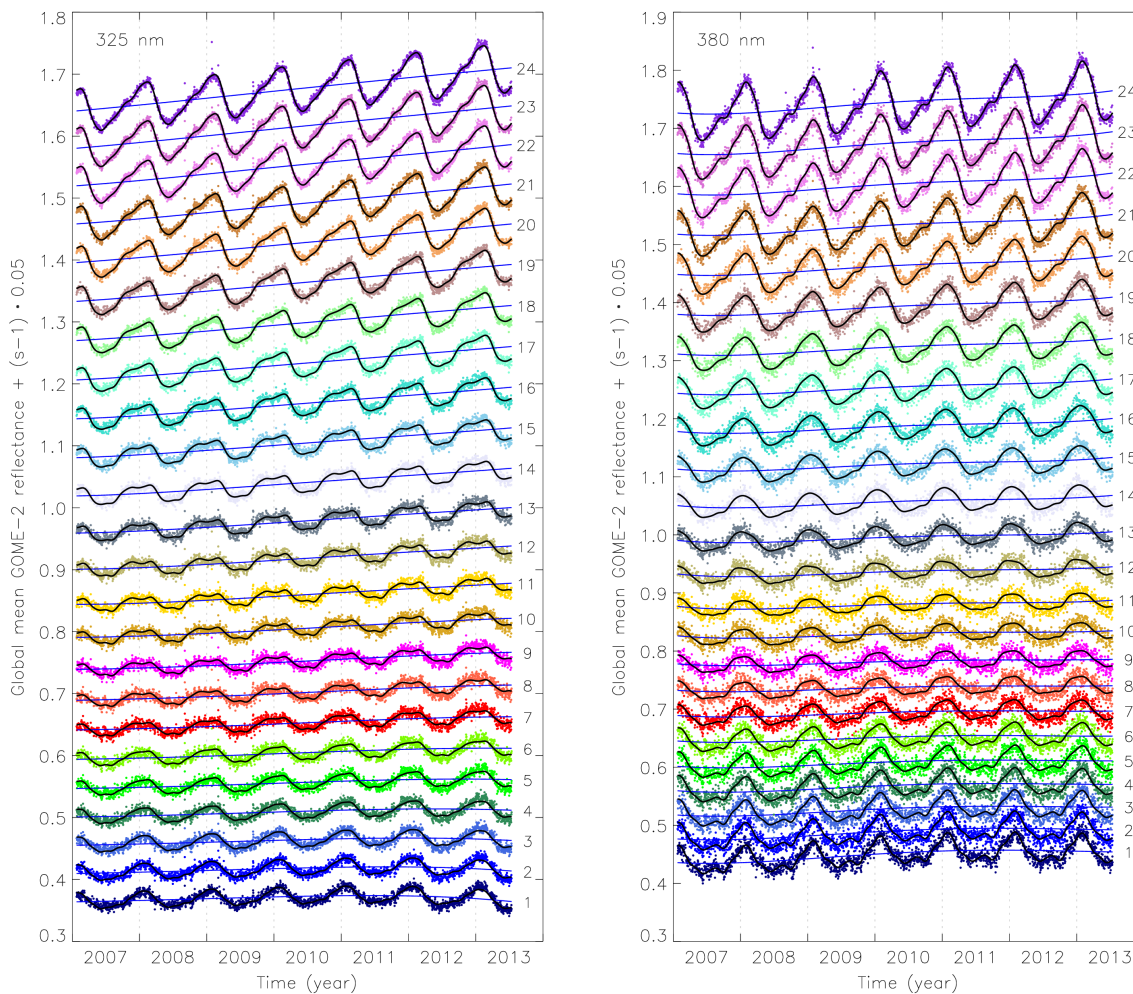


Figure 7: Global mean reflectance measured by GOME-2 at 325 nm (left) and 380 nm (right) as a function of time, for each of the 24 scan mirror positions in the forward scan. To separate the time series graphically, an offset of $(s - 1) \cdot 0.05$ was added to each, where s is the scan mirror position as indicated. The solid black curves are fit results and are described in the main text. The blue monotonous curves illustrate the effect of instrument degradation over the years.

5.3 Correction

The correction for instrument degradation can easily be calculated using

$$c_{\lambda,s}(t) \equiv 1/d_{\lambda,s}(t) = P_{\lambda,s}^{(p)}(0) / P_{\lambda,s}^{(p)}(t) . \quad (10)$$

The measured Earth reflectances have to be multiplied with these correction factors. Note that the global mean reflectances can be calculated directly from the intermediate products “A” (or “B”) in Figure 5. The correction in equation (10) is applied at the beginning of step “4” in Figure 5.

6 Error analysis

The uncertainty on the retrieved surface LER value depends the number of scenes that were selected for the grid cell. If, for instance, the mode of the frequency distribution is selected, there will usually be quite a high number of scenes regarded as representative, and the error on the surface LER will be determined for each wavelength band as the standard deviation in the representative scene LERs. If the 1% cumulative value is used, there are usually less measurements available and the error on the surface LER is a mixture of a predefined error and an error based on the standard deviation. If the retrieved surface LER of the grid cell was based on the minimum scene LER value, then the error is set to a value which depends on the surface type and on the surface LER value itself.

7 Proposed validation

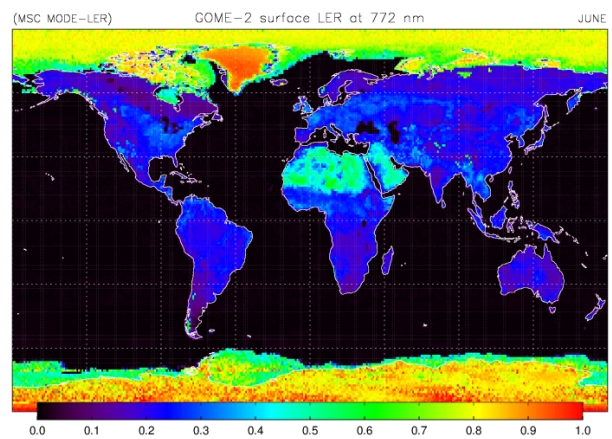
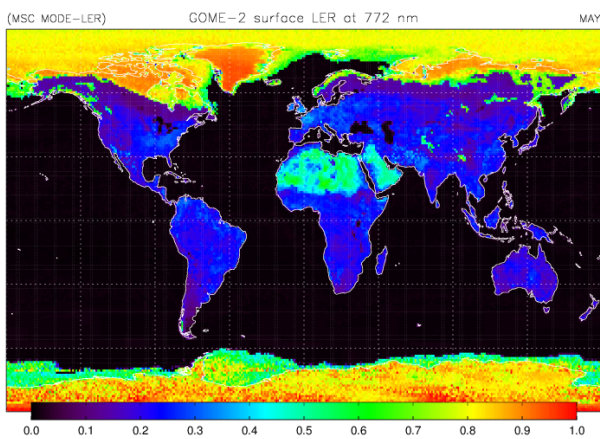
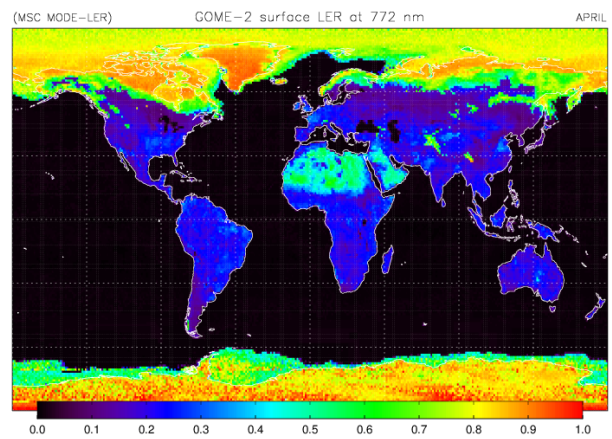
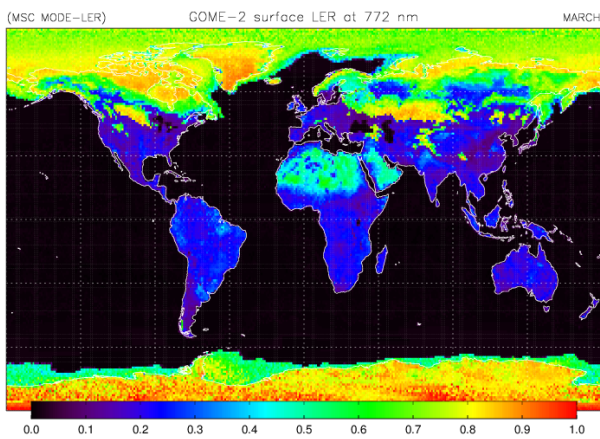
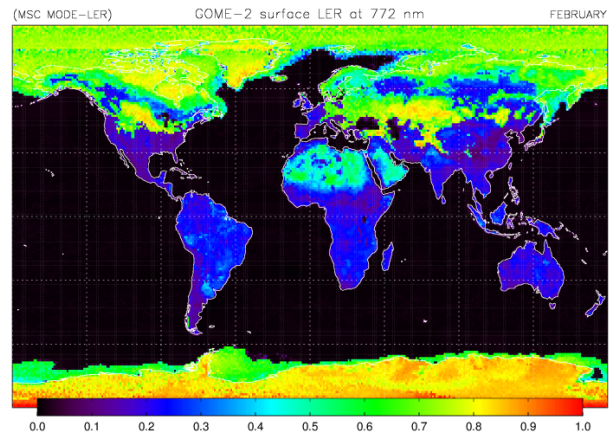
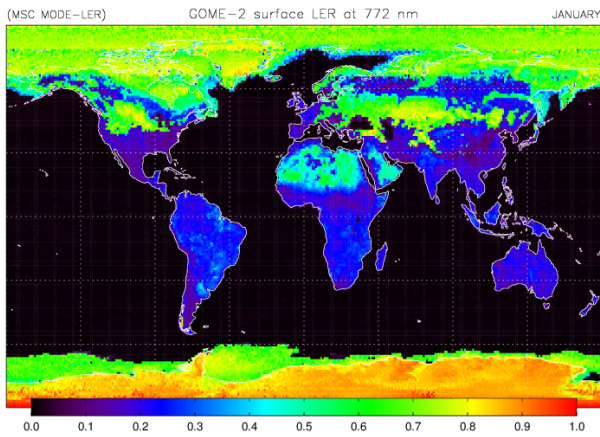
Validation of the retrieved GOME-2 surface LER database may be done by comparison with the other surface LER databases that were discussed in section 2. From these, the GOME surface LER database [Koelemeijer *et al.*, 2003] makes most sense as a reference, because of the orbital and instrumental similarities between GOME and GOME-2, and their overlapping set of LER wavelength bands. Note that the GOME surface LER database was essentially retrieved using the MIN-LER approach (as explained in section 3.3), so a comparison with the GOME surface LER will in principle only allow validation of the GOME-2 surface LER determined using the MIN-LER approach.

The OMI surface LER database [Kleipool *et al.*, 2008] may be used for the wavelengths below 500 nm. The OMI surface LER database is important to have as a reference because it makes use of the same surface LER retrieval approach as the one described in this ATBD. That is, both the GOME-2 MIN-LER and MODE-LER surface LER products can be compared and this will provide information on the correctness of the GOME-2 surface LER algorithm (and products).

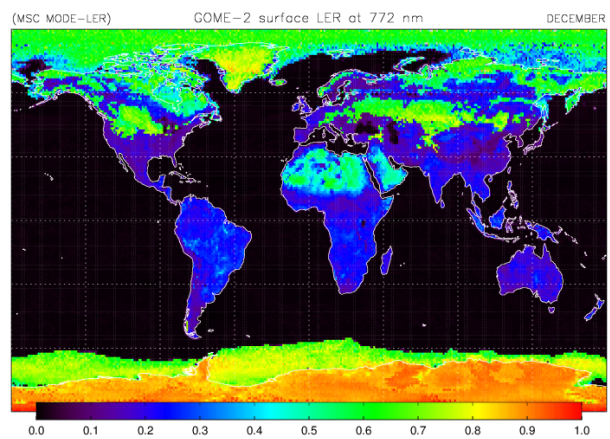
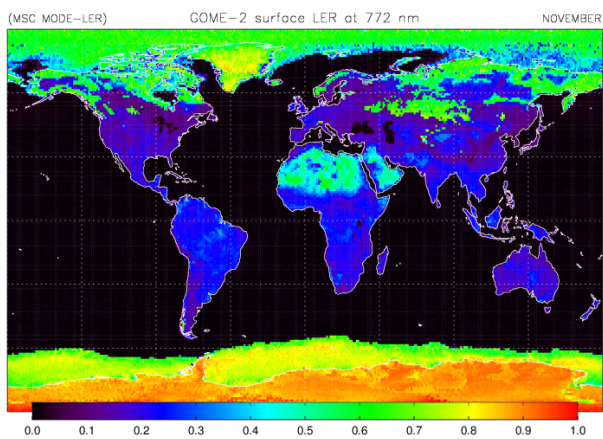
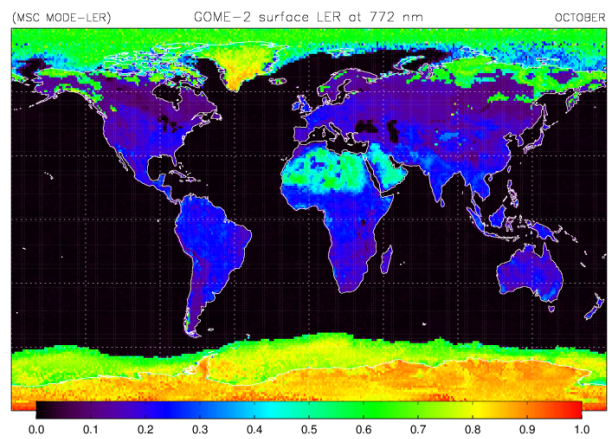
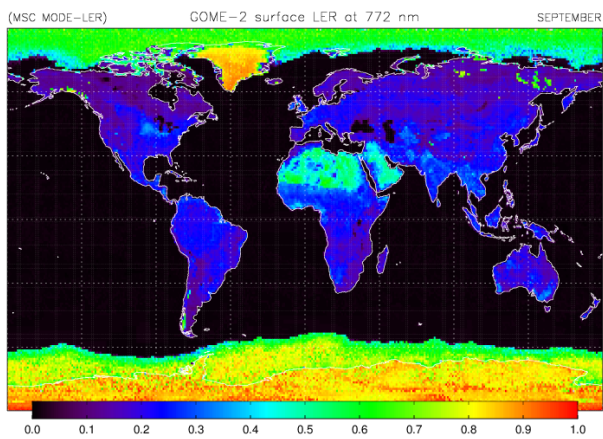
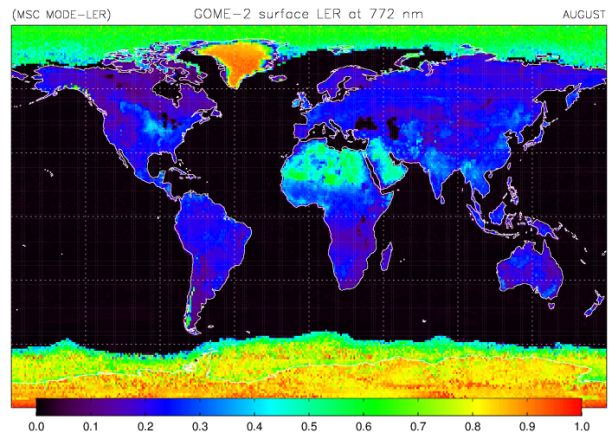
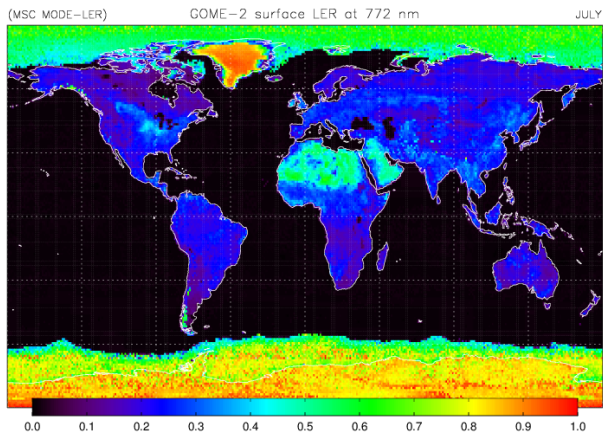
Alternatively, a comparison with non-LER surface albedos, such as the MERIS black-sky albedo (BSA) [Popp *et al.*, 2011], is also possible. This is strictly speaking not correct, because the BSA is the integral of the bidirectional reflectance distribution function (BRDF) over the entire hemisphere whereas the LER is derived from the much smaller range of viewing angles of the satellites observation geometry. Also, the LER approach by definition assumes a direction-independent surface albedo. Nevertheless, a comparison would be feasible and worth the effort. Note that a comparison only makes sense over land, because the MERIS surface LER values over sea are not retrieved from MERIS observations. They were taken directly from the GOME surface LER database.

A Examples of the monthly GOME-2 surface LER product

The following figures present global maps of the GOME-2 surface LER (MODE-LER approach) retrieved at 772 nm for the months January to December. (Continued on next page.)



(Continued from previous page.)



B Overview of solar eclipse events

The following two tables provide an overview of the major solar eclipse events that have occurred since the launch of MetOp-A and MetOp-B. The second column lists the dates on which the solar eclipse events occurred. The third and fourth columns together define the time intervals in which the measurements were noticeably affected. Usually, only one orbit on a day is affected.

satellite	date	start time	end time
MetOp-A	19-03-2007	02:48:52 UTC	03:05:09 UTC
MetOp-A	11-09-2007	12:51:33 UTC	13:07:54 UTC
MetOp-A	07-02-2008	03:11:13 UTC	03:23:38 UTC
MetOp-A	01-08-2008	10:01:38 UTC	10:20:26 UTC
MetOp-A	01-08-2008	15:05:48 UTC	15:13:13 UTC
MetOp-A	26-01-2009	05:55:27 UTC	06:10:45 UTC
MetOp-A	22-07-2009	01:07:56 UTC	01:23:37 UTC
MetOp-A	15-01-2010	05:18:47 UTC	05:33:52 UTC
MetOp-A	11-07-2010	17:49:37 UTC	18:03:43 UTC
MetOp-A	04-01-2011	08:00:51 UTC	08:18:31 UTC
MetOp-A	04-01-2011	09:39:14 UTC	09:48:15 UTC
MetOp-A	25-11-2011	06:38:13 UTC	06:50:19 UTC
MetOp-A	20-05-2012	23:26:31 UTC	23:41:26 UTC
MetOp-A	13-11-2012	21:03:52 UTC	21:23:03 UTC
MetOp-A	09-05-2013	23:16:52 UTC	23:35:22 UTC
MetOp-A	03-11-2013	11:38:12 UTC	11:56:10 UTC

Table 5: Solar eclipse events since the launch of MetOp-A. Given are the date and the time interval in which the measurements were noticeably affected.

satellite	date	start time	end time
MetOp-B	09-05-2013	22:32:29 UTC	22:51:59 UTC
MetOp-B	03-11-2013	10:55:02 UTC	11:04:14 UTC

Table 6: Solar eclipse events since the launch of MetOp-B. Given are the date and the time interval in which the measurements were noticeably affected.

References

- Anderson, G. P., S. A. Clough, F. X. Kneizys, J. H. Chetwynd, and E. P. Shettle (1986), AFGL atmospheric constituent profiles (0–120 km), *Environ. Res. Pap. 954, Rep. AFGL-TR-86-0110*, Air Force Geophys. Lab., Hanscom AFB, Mass.
- Burrows, J. P., et al. (1999), The Global Ozone Monitoring Experiment (GOME): Mission concept and first scientific results, *J. Atmos. Sci.*, 56(2), 151–175.
- Chandrasekhar, S. (1960), *Radiative Transfer*, Dover, Mineola, N. Y., 393p.
- de Haan, J. F., P. B. Bosma, and J. W. Hovenier (1987), The adding method for multiple scattering calculations of polarized light, *Astron. Astrophys.*, 183, 371–391.
- EUMETSAT (2014), GOME-2 Factsheet, Doc. No. EUM/OPS/DOC/10/1299, Issue 4a, 20 May 2014, EUMETSAT, Darmstadt, Germany.
- Heath, D. F., A. J. Krueger, H. A. Roeder, and B. D. Henderson (1975), The Solar Backscatter Ultraviolet and Total Ozone Mapping Spectrometer (SBUV/TOMS) for NIMBUS G, *Opt. Eng.*, 14(4), 144323, doi:10.1117/12.7971839.
- Herman, J. R., and E. A. Celarier (1997), Earth surface reflectivity climatology at 340–380 nm from TOMS data, *J. Geophys. Res.*, 102(D23), 28,003–28,011, doi:10.1029/97JD02074.
- Kleipool, Q. L., M. R. Dobber, J. F. de Haan, and P. F. Levelt (2008), Earth surface reflectance climatology from 3 years of OMI data, *J. Geophys. Res.*, 113, D18308, doi:10.1029/2008JD010290.
- Koelemeijer, R. B. A., J. F. de Haan, and P. Stammes (2003), A database of spectral surface reflectivity in the range 335–772 nm derived from 5.5 years of GOME observations, *J. Geophys. Res.*, 108(D2), 4070, doi:10.1029/2002JD002429.
- Levelt, P. F., G. H. J. van den Oord, M. R. Dobber, A. Mälkki, H. Visser, J. de Vries, P. Stammes, J.O.V. Lundell, and H. Saari (2006), The Ozone Monitoring Instrument, *IEEE Trans. Geosci. Remote Sens.*, 44(5), 1093–1101, doi:10.1109/TGRS.2006.872333.
- Nolin, A. W., R. L. Armstrong, and J. Maslanik (1998), Near-Real-Time SSM/I-SSMIS EASE-Grid Daily Global Ice Concentration and Snow Extent, 2007–2012, National Snow and Ice Data Center, Boulder, Colorado, USA. Digital media, updated daily.
- Popp, C., Wang, P., Brunner, D., Stammes, P., Zhou, Y., and Grzegorski, M. (2011), MERIS albedo climatology for FRESCO+ O2 A-band cloud retrieval, *Atmos. Meas. Tech.*, 4, 463–483, doi:10.5194/amt-4-463-2011.

- Stammes, P. (2001), Spectral radiance modelling in the UV-visible range, in *IRS 2000: Current Problems in Atmospheric Radiation*, edited by W. L. Smith and Y. M. Timofeyev, pp. 385–388, A. Deepak, Hampton, Va.
- Tilstra, L. G., M. de Graaf, I. Aben, and P. Stammes (2012a), In-flight degradation correction of SCIAMACHY UV reflectances and Absorbing Aerosol Index, *J. Geophys. Res.*, *117*, D06209, doi:10.1029/2011JD016957.
- Tilstra, L. G., O. N. E. Tuinder, and P. Stammes (2010), GOME-2 Absorbing Aerosol Index: statistical analysis, comparison to GOME-1 and impact of instrument degradation, in *Proceedings of the 2010 EUMETSAT Meteorological Satellite Conference*, EUMETSAT P.57, ISBN 978-92-9110-089-7, Cordoba, Spain.
- Tilstra, L. G., O. N. E. Tuinder, and P. Stammes (2012b), Introducing a new method for in-flight degradation correction of the Earth reflectance measured by GOME-2, and application to the AAI, in *Proceedings of the 2012 EUMETSAT Meteorological Satellite Conference*, EUMETSAT P.61, Sopot, Poland.
- U.S. Department of Commerce, National Oceanic and Atmospheric Administration, National Geophysical Data Center (2006), *2-minute Gridded Global Relief Data (ETOPO2v2)*, <http://www.ngdc.noaa.gov/mgg/fliers/06mgg01.html>